Inorg. Chem. **2006**, *45*, 8628–8637

Formation of *p*-Phenylenediamine–Crown Ether–$[PMo_{12}O_{40}]^{4-}$ Salts

Tomoyuki Akutagawa,*[†,‡,§] Daigoro Endo,[‡] Hiroyuki Imai,[||] Shin-ichiro Noro,[†,‡] Leroy Cronin,[⊥] and Takayoshi Nakamura*[†,‡,§]

Research Institute for Electronic Science, Hokkaido University, Sapporo 060-0812, Japan, Graduate School of Environmental Earth Science, Hokkaido University, Sapporo 060-0810, Japan, CREST, Japan Science and Technology Agency (JST), Kawaguchi 332-0012, Japan, Venture Business Laboratory, Hokkaido University, Sapporo 060-8628, Japan, and WestCHEM, Department of Chemistry, University of Glasgow, Glasgow G12 8QQ, U.K.

Received May 18, 2006

Electron transfer from the electron donor of *p*-phenylenediamine (PPD) to the electron acceptor of $(H^+)_3[PMo_{12}O_{40}]^{3-}$ forms a one-electron-reduced Keggin cluster of $[PMo_{12}O_{40}]^{4-}$, bearing a $S = {}^1/_2$ spin, while proton transfer from the proton donor of $(H^+)_3[PMo_{12}O_{40}]^{3-}$ to the proton acceptor of PPD yielded mono- and diprotonated cations of 4-aminoanilinium ($HPPD^+$) and *p*-phenylenediammonium ($H2PPD^{2+}$). By introduction of crown ether receptors during the crystallization process, supramolecular cations of ($HPPD^+$)(crown ethers) and/or (H_2PPD^{2+})(crown ethers) were successfully introduced into three new α-$[PMo_{12}O_{40}]^{4-}$ salts of $(H_2PPD^{2+})_2$([12]crown-4)$_4[PMo_{12}O_{40}]^{4-}$ (**1**), $(HPPD^+)_4$-([15]crown-5)$_4[PMo_{12}O_{40}]^{4-}$ (**2**), and $(HPPD^+)_2(H_2PPD^{2+})$([18]crown-6)$_4[PMo_{12}O_{40}]^{4-}$ (**3**) as the countercation. The protonated states of PPD and molecular-assembly structures of the supramolecular cations depended on the size of the crown ethers. In salt **3**, a novel mixed-protonated state of $HPPD^+$ and H_2PPD^{2+} was confirmed to be complexed in the cation structure. According to the changes in the cation structures, the anion arrangements were modulated from those of the two-dimensional layer for salt **1** to the isolated cluster for salts **2** and **3**. The temperature-dependent magnetic susceptibilities of salts **1**–**3** were consistent with the isolated spin arrangements of $[PMo_{12}O_{40}]^{4-}$. The electronic spectra of salts **1**–**3** indicated the intervalence optical transition from pentavalent Mo^V to hexavalent Mo^{VI} ions within the $[PMo_{12}O_{40}]^{4-}$ cluster. Temperature-dependent electron spin resonance spectra of salt **2** revealed the delocalization–localization transition of the $S = {}^1/_2$ spin at 60 K. The spin on the $[PMo_{12}O_{40}]^{4-}$ cluster was localized on a specific Mo^V site below 60 K, which was thermally activated with an activation energy of 0.015 eV.

Introduction

Polyoxomolybdates (POMs) such as $[Mo_6O_{19}]$, $[Mo_8O_{26}]$, $[Mo_{10}O_{36}]$, and $[PMo_{12}O_{40}]$ are synthesized by condensation reactions of molybdic acid derivatives under acidic conditions.[1,2] The combination of corner-, edge-, and face-sharing $[MoO_x]$ units (where $x = 4, 6, 7$) can yield a vast structural diversity of the POMs. Among them, the compound α-$[PMo_{12}O_{40}]$, which displays the archetypal Keggin structure, was the first POM reported by Berzelius in 1826 and has been extensively examined from the viewpoints of catalysis,[3] antiviral activity,[4] gas adsorption,[5] and electronic[6,7] and magnetic[8] materials. The molecular structure of α-$[PMo_{12}O_{40}]$ is constructed from the corner-sharing of 12

* To whom correspondence should be addressed. E-mail: takuta@imd.es.hokudai.ac.jp (T.A.), tnaka@imd.es.hokudai.ac.jp (T.N.). Phone: +81-11-706-2884. Fax: +81-11-706-4972.

[†] Research Institute for Electronic Science, Hokkaido University.

[‡] Graduate School of Environmental Earth Science, Hokkaido University.

[§] CREST, Japan Science and Technology Agency.

[||] Venture Business Laboratory, Hokkaido University.

[⊥] University of Glasgow.

(1) (a) *Polyoxometalate Molecular Science*; Borrás-Almenar, J. J., Coronado, E., Müller, A., Pope, M., Eds.; Kluwer Academic Publishers: London, 2001. (b) *Polyoxometalate Chemistry From Topology via Self-Assembly to Applications*; Pope, T., Müller, A., Eds.; Kluwer Academic Publishers: London, 2001. (c) *Polyoxometalate Chemistry for Nano-Composite Design*; Yamase, T., Pope, M. T., Eds.; Kluwer Academic Publishers: New York, 2002. (d) Cronin, L. High Nuclearity Polyoxometalate Clusters. *Compr. Coord. Chem. II* **2004**, *7*, 1.

(2) (a) Müller, A.; Kögerler, P.; Kuhlmann, C. *Chem. Commun.* **1997**, 1437. (b) Müller, A.; Kögerler, P.; Dress, A. W. M. *Coord. Chem. Rev.* **2001**, *222*, 193. (c) Müller, A.; Serani, C. *Acc. Chem. Res.* **2000**, *32*, 2. (d) Müller, A.; Roy, S. *Coord. Chem. Rev.* **2003**, *245*, 153.

(3) References were cited in: (a) Kozhevnikov, I. V. *Chem. Rev.* **1998**, *98*, 171. (b) Mizuno, N.; Misono, M. *Chem. Rev.* **1998**, *98*, 199.

(4) References were cited in: Rhule, J. T.; Hill, C. L.; Judd, D. A. *Chem. Rev.* **1998**, *98*, 327.

(5) Ishi, Y.; Takenaka, Y.; Konishi, K. *Angew. Chem., Int. Ed.* **2004**, *43*, 2702.

10.1021/ic060857i CCC: $33.50
Published on Web 09/14/2006

$[MoO_6]$ octahedra, and the central PO_4^{3-} anion is included at the center of the cluster.[1] Three types of O atoms are present in the α-Keggin structure, and these can be identified as terminal Mo−O, bridging Mo−O−Mo, and anionic P−O species. Because each Mo ion is coordinated by six O atoms in an octahedral fashion, the energy levels of the 4d orbitals on the Mo ions are split into t_{2g} and e_g orbitals. Therefore, it is not a surprise that multistep redox properties are one of the most notable properties of the Mo-based α-Keggin. The α-$[PMo_{12}O_{40}]^{3-}$, one-electron-reduced α-$[PMo_{12}O_{40}]^{4-}$, and two-electron-reduced α-$[PMo_{12}O_{40}]^{5-}$ species, with the α-Keggin structure, have been characterized in the solid state, while the rearrangement of the three-electron-reduced α-$[PMo_{12}O_{40}]^{6-}$ to the lacunary $[PMo_{11}O_{39}]^{6-}$ compound is facile.[1a] Although the α-$[PMo_{12}O_{40}]^{3-}$ cluster is electrically and magnetically inert because of the $(4d)^0$ electronic structure of all 12 Mo^{VI} ions, the one-electron-reduced $[PMo_{12}O_{40}]^{4-}$ species with one pentavalent Mo^V ion of the $(4d)^1$ electronic structure is electrically and magnetically active.[6−8] Indeed, it has been shown that the mixed-valence electronic structure of $[PMo^{V}Mo^{VI}{}_{11}O_{40}]^{4-}$ gives rise to the intervalence optical transition from pentavalent Mo^V to hexavalent Mo^{VI} within the cluster, and temperature-dependent electron spin resonance (ESR) spectra reveal a localization−delocalization spin transition.[9] As such, it can be seen that the dynamic properties of electron and spin in the mixed-valence POM system are interesting from the point of view of constructing novel electronic and magnetic materials.[10]

In this context, we have been introducing supramolecular cation structures between inorganic or organic cations and crown ethers as the countercations of $[Ni(dmit)_2]$ ($dmit^{2-}$ = 2-thioxo-1,3-dithiole-4,5-dithiolate).[11−13] This approach allows us to modify and modulate the assembled structures of the $[Ni(dmit)_2]^-$ anions in the crystal and thus to modify the magnetic properties of the $[Ni(dmit)_2]^-$ salts.[12] By using this approach, relatively large and complex cations, which consist of an organic ammonium cation such as anilinium and *p*-phenylenediammonium (H_2PPD^{2+}), with crown ethers were also introduced into the crystal, which gave rise to a spin ladder of interactions of $S = {}^1/_2$ spin on $[Ni(dmit)_2]^-$ anions.[13] However, the $[Ni(dmit)_2]^-$ anions are relatively small for embedding large and structurally diverse supramolecular cations in the crystal lattice. Therefore, in the present study, we used the Keggin cluster as a counteranion of the supramolecular cations [these supramolecular cations are comprised of the 4-aminoanilinium ($HPPD^+$) or H_2PPD^{2+} complex via H-bonded interactions to the cavity of the crown ether]. In the course of crystallization, both the electron- and proton-transfer processes between the electron donor (proton acceptor) of *p*-phenylenediamine (PPD) and electron acceptor (proton donor) of $(H^+)_3[PMo_{12}O_{40}]^{3-}$ yield the H-bonded supramolecular cations and the one-electron-reduced $[PMo_{12}O_{40}]^{4-}$ in the crystal. The two $-NH_2$ sites of the PPD molecule have the potential to form two kinds of cations of $HPPD^+$ and H_2PPD^{2+} via a proton-accepting process according to the reaction between PPD and $(H^+)_3[PMo_{12}O_{40}]^{3-}$ in solution. When the acid-dissociation constant of $(H^+)_3[PMo_{12}O_{40}]^{3-}$ is lower than that of PPD, complete proton transfer from $(H^+)_3[PMo_{12}O_{40}]^{3-}$ to PPD occurs, giving rise to the dication, H_2PPD^{2+}, during the crystallization process.[14,15] Because the crown ether moiety has a much higher affinity for the cationic $-NH_3^+$ group than the neutral $-NH_2$ group,[16] both the size and shape of the supramolecular assemblies between $HPPD^+$ or H_2PPD^{2+} and crown ethers are strongly affected by the proton-transfer state of PPD.

(6) (a) Abbas, H.; Pickering, A. L.; Long, D.; Kögerler, P.; Cronin, L. *Chem.−Eur. J.* **2005**, *11*, 1071. (b) Clemente-León, M.; Coronado, E.; Gómez-Garcia, C. J.; Mingotaud, C.; Ravaine, S.; Romualdo-Torres, G.; Delhaès, P. *Chem.−Eur. J.* **2005**, *11*, 3979.

(7) (a) Ouahab, L.; Grandjean, D.; Bencharif, M. *Acta Crystallogr., Sect. C* **1991**, *47*, 2670. (b) Ouahab, L.; Bencharif, M.; Mhanni, A.; Pelloquin, D.; Halet, J.-F.; Peña, O.; Padiou, J.; Grandjean, D.; Garrigou-Lagrange, C.; Amiell, J.; Delhaes, P. *Chem. Mater.* **1992**, *4*, 666. (c) Maguerès, P. L.; Ouahab, L.; Golhen, S.; Grandjean, D.; Pena, O.; Jegaden, J.-C.; Gómez-Garcia, C. J.; Delhaès, P. *Inorg. Chem.* **1994**, *33*, 5180. (d) Gómez-Garcia, C. J.; Ouahab, L.; Gimenéz-Saiz, C.; Triki, S.; Coronado, E.; Delhaès, P. *Angew. Chem., Int. Ed. Engl.* **1994**, *33*, 223. (e) Galan-Mascarós, J. R.; Gimenéz-Saiz, C.; Triki, S.; Gómez-Garcia, J.; Coronado, E.; Ouahab, L. *Angew. Chem., Int. Ed. Engl.* **1995**, *34*, 1460. (f) Bellitto, C.; Bonamico, M.; Fares, V.; Federici, F.; Righini, G.; Kurmoo, M.; Day, P. *Chem. Mater.* **1995**, *7*, 1475. (g) Coronado, E.; Galan-Mascarós, J. R.; Gimenéz-Saiz, C.; Gómez-Garcia, C. J.; Triki, S. *J. Am. Chem. Soc.* **1998**, *120*, 4671. (h) Coronado, E.; Galan-Mascarós, J. R.; Gimenéz-Saiz, C.; Gómez-Garcia, C. J.; Falvello, L. R.; Delhaès, P. *Inorg. Chem.* **1998**, *37*, 2183. (i) Coronado, E.; Gómez-Garcia, C. J. *Chem. Rev.* **1998**, *98*, 273. (j) Coronado, E.; Giménez-Saiz, C. J.; Gómez-Garcia, C. J.; Capelli, S. J. *Angew. Chem., Int. Ed.* **2004**, *43*, 3022. (k) Nyman, M.; Ingersoll, D.; Singh, S.; Bonhomme, F.; Alam, T. M.; Brinker, C. J.; Rodriguez, M. A. *Chem. Mater.* **2005**, *17*, 2885. (l) Coronado, E.; Galán-Mascarós, J. R.; Giménez-Saiz, C.; Gómez-García, C. J.; Martínez-Ferrero, E.; Almeida, M.; Lopes, E. B.; Capelli, S. C.; Llusar, R. M. *J. Mater. Chem.* **2004**, *14*, 1867.

(8) (a) Müller, A.; Peters, F.; Pope, M. T.; Gatteschi, D. *Chem. Rev.* **1998**, *98*, 239. (b) Gatteschi, D.; Pardi, L.; Barra, A. L.; Müller, A.; Döring, J. *Nature* **1991**, *354*, 463.

(9) (a) Prados, R. A.; Meiklejohn, P. T.; Pope, M. T. *J. Am. Chem. Soc.* **1974**, *96*, 1261. (b) Prados, R. A.; Pope, M. T. *Inorg. Chem.* **1976**, *15*, 2547. (c) Sanchez, C.; Livage, J.; Launary, J. P.; Fournier, M.; Jeannin, Y. *J. Am. Chem. Soc.* **1982**, *104*, 3194.

(10) Suaud, N.; Gaita-Ariño, A.; Clemente-Juan, J. M.; Coronado, E. *Chem.−Eur. J.* **2004**, *10*, 4041.

(11) (a) Nakamura, T.; Akutagawa, T.; Honda, K.; Underhill, A. E.; Coomber, A. T.; Friend, R. H. *Nature* **1998**, *394*, 159. (b) Akutagawa, T.; Nezu, Y.; Hasegawa, T.; Nakamura, T.; Sugiura, K.; Sakata, Y.; Inabe, T.; Underhill, A. E. *Chem. Commun.* **1998**, 2599. (c) Akutagawa, T.; Hasegawa, T.; Nakamura, T.; Takeda, S.; Inabe, T.; Sugiura, K.; Sakata, Y.; Underhill, A. E. *Inorg. Chem.* **2000**, *39*, 2645. (d) Akutagawa, T.; Hasegawa, T.; Nakamura, T.; Takeda, S.; Inabe, T.; Sugiura, K.; Sakata, Y.; Underhill, A. E. *Chem.−Eur. J.* **2001**, *7*, 4902. (e) Akutagawa, T.; Hasegawa, T.; Nakamura, T.; Inabe, T. *J. Am. Chem. Soc.* **2002**, *124*, 8903.

(12) (a) Takamatsu, N.; Akutagawa, T.; Hasegawa, T.; Nakamura, T.; Inabe, T.; Fujita, W.; Awaga, K. *Inorg. Chem.* **2000**, *39*, 870. (b) Akutagawa, T.; Nishihara, S.; Takamatsu, N.; Hasegawa, T.; Nakamura, T.; Inabe, T. *J. Phys. Chem. B* **2000**, *104*, 5871. (c) Akutagawa, T.; Takamatsu, N.; Shitagami, K.; Hasegawa, T.; Nakamura, T.; Inabe, T. *J. Mater. Chem.* **2001**, *11*, 2118. (d) Akutagawa, T.; Hashimoto, A.; Nishihara, S.; Hasegawa, T.; Nakamura, T. *J. Supramol. Chem.* **2002**, *2*, 175. (e) Akutagawa, T.; Hashimoto, A.; Nishihara, S.; Hasegawa, T.; Nakamura, T. *J. Phys. Chem. B* **2003**, *107*, 66. (f) Nishihara, T.; Akutagawa, T.; Hasegawa, T.; Nakamura, T. *Inorg. Chem.* **2003**, *42*, 2480. (g) Akutagawa, T.; Shitagami, K.; Nishihara, S.; Takeda, S.; Hasegawa, T.; Nakamura, T.; Hosokoshi, Y.; Inoue, K.; Ikeuchi, S.; Miyazaki, Y.; Saito, K. *J. Am. Chem. Soc.* **2005**, *127*, 4397. (h) Ikeuchi, S.; Miyazaki, Y.; Takeda, S.; Akutagawa, T.; Nishihara, S.; Nakamura, T.; Saito, K. *J. Chem. Phys.* **2005**, *123*, 044514.

(13) (a) Nishihara, S.; Akutagawa, T.; Hasegawa, T.; Nakamura, T. *Chem. Commun.* **2002**, 408. (b) Nishihara, S.; Akutagawa, T.; Hasegawa, T.; Fujiyama, S.; Nakamura, T.; Nakamura, T. *J. Solid State Chem.* **2002**, *168*, 661.

(14) Kozhevnikov, I. V. *Chem. Rev.* **1998**, *98*, 171.

(15) *Handbook of Chemistry and Physics*, 83rd ed.; CRC Press: New York, 2002.

Chart 1. Molecular Structures of PPD, Crown Ethers, and $[PMo_{12}O_{40}]$

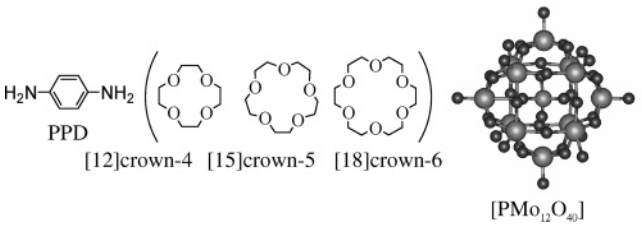

Also, the change in the cation structure will modify the arrangement of the $[PMo_{12}O_{40}]^{4-}$ cluster in the crystalline state. We examined the combination of supramolecular cations between protonated PPDs and crown ethers by changing the size of the crown ethers from [12]crown-4, to [15]crown-5, to [18]crown-6 and obtained the single crystals of $(H_2PPD^{2+})_2$([12]crown-4)$_4[PMo_{12}O_{40}]^{4-}$ (**1**), $(HPPD^+)_4$([15]crown-5)$_4[PMo_{12}O_{40}]^{4-}$ (**2**), and mixed-protonated $(HPPD^+)_2(H_2PPD^{2+})$([18]crown-6)$_3[PMo_{12}O_{40}]^{4-}$ $(CH_3CN)_4$ (**3**) (Chart 1). Herein, we report the preparation and structural, optical, and magnetic properties of three new Keggin salts, in which different types of protonated states of PPD derivatives afforded unique supramolecular structures.

Experimental Section

Preparation of One-Electron-Reduced $[PMo_{12}O_{40}]^{4-}$ Salts. $(H^+)_3[PMo_{12}O_{40}]\cdot nH_2O$ ($n = 20$) and *p*-phenylenediamine (PPD) purchased from Tokyo Kasei Inc. were used without further purification. The crystals were grown using standard diffusion methods in an H-shaped cell (~50 mL).[17] $(H^+)_3[PMo_{12}O_{40}]\cdot nH_2O$ (~100 mg) and PPD (50 mg)−crown ethers (200 mg) were introduced into opposite sides of the H-shaped cell, and CH_3CN (distilled prior to use) was introduced into the diffusion cell slowly. After 10 days, single crystals with typical dimensions of 0.5 × 0.5 × 0.4 mm^3 were obtained as black blocks. Yields of salts **1**−**3** were 42, 35, and 39%, respectively. The stoichiometry of the compound was determined by X-ray structural analysis and elemental analysis. Elem anal. Calcd for $C_{44}H_{84}O_{56}N_4Mo_{12}P$ (salt **1**): C, 19.24; H, 3.08; N, 2.04. Found. C, 19.30; H, 2.92; N, 2.10. Calcd for $C_{64}H_{116}O_{60}N_8Mo_{12}P$ (salt **2**): C, 24.48; H, 3.72; N, 3.57. Found. C, 24.60; H, 3.60; N, 3.94. Calcd for $C_{74}H_{138}O_{64}N_{10}Mo_{12}P$ (salt **3**): C, 26.34; H, 4.12; N, 4.15. Found. C, 25.81; H, 3.78; N, 4.06. The solvent content (CH_3CN) in salt **3** was determined by thermogravimetric−differential thermal analysis (TG−DTA) measurement using a Rigaku Thermo Plus TG8120 with a scanning rate of 5 K min^{-1} under a N_2 flow. These measurements showed a ca. 4% weight loss up until 413 K, which indicates that four CH_3CH solvent molecules are present in **3**.

Cyclic Voltammetry. The redox potentials of PPD and $(n\text{-}Bu_4N)_3[PMo_{12}O_{40}]^{3-}$ were measured in anhydrous CH_3CN with 0.1 M $(n\text{-}Bu_4N)(BF_4)$ as the supporting electrolyte, using Pt electrodes (working and counter electrodes) and a saturated calomel electrode (SCE) as the reference electrode. The scan rate was 20 mV s^{-1}. $(n\text{-}Bu_4N)_3[PMo_{12}O_{40}]^{3-}$ was prepared by a cation-exchange reaction according to the literature.[9a]

Crystal Structure Determination. Crystallographic data (Table 1) were collected by a Rigaku Raxis-Rapid diffractometer using Mo Kα ($\lambda = 0.710\ 73$ Å) radiation from a graphite monochromator. Structural refinements were performed using the full-matrix least-squares method on F^2. Calculations were performed using *Crystal Structure* software packages.[18] Parameters were refined using anisotropic temperature factors except for the H atoms, and these were refined using the riding model with a fixed C−H distance of 0.95 Å.

Optical Spectra. Infrared (IR; 400−7600 cm^{-1}) spectral measurements were carried out using KBr disks on a Perkin-Elmer Spectrum 2000 spectrophotometer with a resolution of 2 cm^{-1}. UV−vis−near-IR spectra (350−3200 nm) were measured on KBr disks using a Perkin-Elmer Lambda-19 spectrophotometer with a resolution of 2 nm. Raman measurements where made using a Jasco RMP-210S microscope with an Ar-laser excitation source at 532 nm. The Stokes shift from the surface of single crystals was detected in a backscattering detector arrangement.

Magnetic Susceptibility. The magnetic susceptibility was measured using a Quantum Design model MPMS-5 SQUID magnetometer for polycrystalline samples. The applied magnetic field was 1 T for all measurements.

ESR. Temperature-dependent ESR spectra were measured using a JEOL JES FA-100 spectrometer equipped with a temperature control system (Oxford ESR900 cryostat). The single crystals were attached to a support on a quartz sample holder. The *g* values of the ESR signals were corrected at the third and fourth reference signals of MnO. All ESR signals were fitted using the Lorentzian line shape.

Results and Discussion

Preparation of Salts 1−3. The stoichiometries and protonation states of PPD derivatives for salts **1**−**3** were determined as $(H_2PPD^{2+})_2$([12]crown-4)$_4[PMo_{12}O_{40}]^{4-}$ (**1**), $(HPPD^+)_4$([15]crown-5)$_4[PMo_{12}O_{40}]^{4-}$ (**2**), and $(HPPD^+)_2(H_2PPD^{2+})$([18]crown-6)$_4[PMo_{12}O_{40}]^{4-}(CH_3CN)_4$ (**3**), from the elemental analysis, X-ray crystal structural analysis, and IR spectra. The changes in the protonated states of PPD modified the structures of the supramolecular cations and cluster arrangements (see below). Further, the absolute magnitude of the magnetic susceptibilities of salts **1**−**3** were in accordance with the formation of the one-electron-reduced $[PMo_{12}O_{40}]^{4-}$ species. Although one electron was transferred from PPD to $[PMo_{12}O_{40}]^{3-}$ during the formation of the crystal lattice, no oxidized species of PPD were included in the structure. However, protons were transferred from $H^+_3[PMo_{12}O_{40}]^{3-}$ to PPD, which generated $HPPD^+$ or H_2PPD^{2+} in $[PMo_{12}O_{40}]^{4-}$ via complexation with the crown ether moieties. Slow diffusion between $(H^+)_3[PMo_{12}O_{40}]^{3-}$ and PPD−crown ethers in CH_3CN yielded both the proton- and electron-transferred states in salts **1**−**3**. We discuss the crystal formation from the viewpoints of electron- and proton-transfer processes in solution.[19,20]

Upon crystallization, the color of the mother liquor changed from yellow to black-violet by the slow diffusion

(16) (a) Izatt, R. M.; Bradshaw, J. S.; Nielsen, S. A.; Lamb, J. D.; Christensen, J. J.; Sen, D. *Chem. Rev.* **1985**, *85*, 271. (b) Izatt, R. M.; Pawlak, K.; Bradshaw, J. D.; Bruening, R. L. *Chem. Rev.* **1991**, *91*, 721.

(17) Nirgey, P. *J. Cryst. Growth* **1977**, *40*, 265.

(18) *Crystal Structure: Single-crystal structure analysis software*, version 3.6; Rigaku Corp. & Molecular Structure Corp.: The Woodlands, TX, 2004.

(19) (a) Sadakane, M.; Steckhan, E. *Chem. Rev.* **1998**, *98*, 219. (b) Himeno, S.; Takamoto, M.; Santo, R.; Ichimura, A. *Bull. Chem. Soc. Jpn.* **2005**, *78*, 95.

Table 1. Selected Crystal Parameter of Salts **1**−**3**

	1	**2**	**2**	**3**
empirical formula	$C_{44}H_{84}O_{56}N_4Mo_{12}P$	$C_{64}H_{116}O_{60}N_8Mo_{12}P$	$C_{64}H_{116}O_{60}N_8Mo_{12}P$	$C_{74}H_{138}N_{10}O_{64}Mo_{12}P$
fw	1373.70	1569.95	1569.95	1687.09
space group	$P\bar{1}$ (No. 2)	$P\bar{1}$ (No. 2)	$P\bar{1}$ (No. 2)	$P\bar{1}$ (No. 2)
a, Å	12.07(4)	13.74(3)	13.59(3)	14.241(6)
b, Å	13.15(3)	14.52(2)	14.57(3)	14.617(5)
c, Å	14.45(4)	16.26(3)	16.16(3)	14.878(6)
α, deg	82.65(8)	65.13(6)	64.74(6)	102.68(1)
β, deg	68.75(9)	64.74(6)	65.32(6)	91.73(2)
γ, deg	65.81(9)	67.12(6)	67.15(7)	105.29(2)
V, Å^3	1949(9)	2573(8)	2543(8)	2901(2)
Z	1	1	1	1
D_{calc}, g cm^{-3}	2.340	2.026	2.050	1.931
μ, cm^{-1}	19.905	15.258	15.437	13.632
T, K	298	298	100	100
no. of reflns measd	17 719	40 485	37 743	27 848
no. of indep reflns used	5898	22 278	7607	9286
$\sigma(I)$	0.3	2.5	1.5	2.0
R^a	0.060	0.043	0.045	0.038
$R_w(F^2)^a$	0.144	0.064	0.053	0.062
GOF	1.29	1.14	1.14	1.09

[a] $R = \sum||F_o| - |F_c||/\sum|F_o|$ and $R_w = [\sum(\omega(F_o^2 - F_c^2)^2)/\sum\omega(F_o^2)^2]^{1/2}$.

of $(H^+)_3[PMo_{12}O_{40}]^{3-}$ and PPD in CH_3CN over 2−3 days, and then black single crystals of salts **1**−**3** were obtained as one-electron-reduced mixed-valence $[PMo_{12}O_{40}]^{4-}$ salts. Because the crown ethers are electrochemically inert, electron transfer from the electron donor of PPD to the electron acceptor of $[PMo_{12}O_{40}]^{3-}$ yielded the one-electron-reduced $[PMo_{12}O_{40}]^{4-}$ state. The electron-accepting and -donating abilities of $[PMo_{12}O_{40}]^{3-}$ and PPD were evaluated from cyclic voltammetry in CH_3CN.[19] Reversible two-step, one-electron reduction of $[PMo_{12}O_{40}]^{3-}$ were observed at the half-wave reduction potentials of $E^r_{1/2}(1) = +0.394$ V and $E^r_{1/2}(2) = +0.051$ V, respectively (vs SCE, *n*-Bu_4NBF_4, Pt in CH_3CN). The $E^r_{1/2}(1)$ values of strong electron acceptors of 7,7,8,8-tetaracyano-*p*-quinodimethane (TCNQ) and 2,5-difluoro-TCNQ (F_2-TCNQ) were observed at $E_{1/2}(1) = +0.421$ and +0.231 V, respectively. Therefore, the strength as an electron acceptor of $[PMo_{12}O_{40}]^{3-}$ was higher than that of TCNQ and similar to that of F_2-TCNQ, suggesting that the electron-accepting ability was high enough to cause the electron transfer from typical electron donors to $[PMo_{12}O_{40}]^{3-}$ in CH_3CN. Also, the half-wave first oxidation potential $[E^o_{1/2}(1)]$ of PPD was observed at +0.803 V under the same measurement conditions. The ability of electron transfer from PPD to $[PMo_{12}O_{40}]^{3-}$ was estimated from the difference of the redox potentials between $E^o_{1/2}(1)$ of PPD and $E^r_{1/2}(1)$ of $[PMo_{12}O_{40}]^{-3}$ [$\Delta E = E^o_{1/2}(1) - E^r_{1/2}(1) = +0.41$ V], the value of which was within the range expected for the formation of ionic electronic ground state of $(PPD^+)-[PMo_{12}O_{40}]^{4-}$.[21] The electron-donating and -accepting abilities of PPD and $[PMo_{12}O_{40}]^{3-}$ were appropriate to form a completely electron-transferred ionic ground state of the donor−acceptor-type charge-transfer system, although the cation radicals of PPD or their protonated species were not incorporated into the crystals.

The highly acidic properties of $(H^+)_3[PMo_{12}O_{40}]^{3-}$ have been reported in solution,[14] and the monoprotonated $HPPD^+$ state can be expected to coexist in equilibrium with H_2PPD^{2+} under the crystallization conditions because both $HPPD^+$ and H_2PPD^{2+} have the possibility of being included as countercations of the $[PMo_{12}O_{40}]^{4-}$ anion species. [12]crown-4, [15]crown-5, and [18]crown-6 formed supramolecular cations with appropriate cationic species of $HPPD^+$ and/or $H2PPD^{2+}$ in order to fit the overall cation such that closely packed crystal structures of salts **1**−**3** were realized.

Crystal Structures of Salts 1−3. The cluster frameworks $[PMo_{12}O_{40}]^{4-}$ found in salts **1**−**3** were found to adopt the α-Keggin structure, such that the asymmetric unit is comprised of half of the $[PMo_{12}O_{40}]^{4-}$ unit. Furthermore, the central PO_4^{3-} anion was found to be disordered over two positions with equal probability at both 298 and 100 K.

Supramolecular Cation Structures. Overall, the molecular assemblies of the protonated PPD−crown ethers in salts **1**−**3** are quite distinct from each other (Figure 1). A largely deformed sandwich-type cation structure of $(H2PPD^{2+})([12]\text{-crown-4})_2$ was observed in salt **1** (Figure 1a), in which eight O atoms of upper and lower [12]crown-4 molecules are interacting with the two $-NH_3^+$ groups of the H_2PPD^{2+} dication through $N-H^+\sim O$ hydrogen-bonded interactions.

Two kinds of crystallographically independent cation structures of $HPPD^+$([15]crown-5), A and B units, were observed in salt **2** (Figure 1b). At 298 K, positional disorder of the C atoms in $HPPD^+$ was observed in the A unit, while one orientation was identified in the crystal structure of the A unit at 100 K (Figures S4 and S5 of the Supporting Information). The average thermal parameter of the C atoms of $HPPD^+$ in the A unit ($B_{eq} = 12.4$) was ca. 3 times larger than that in the B unit ($B_{eq} = 4.2$) at 100 K, and the molecular packing of $HPPD^+$ in the A unit was much looser than that in the B unit. The result strongly suggested that the rotation of the phenyl ring around the long axis of $HPPD^+$ is expected

(20) (a) Akutagawa, T.; Saito, G. *Bull. Chem. Soc. Jpn.* **1995**, *68*, 1753. (b) Akutagawa, T.; Saito, G.; Kusunoki, M.; Sakaguchi, K. *Bull. Chem. Soc. Jpn.* **1996**, *69*, 2487. (c) Akutagawa, T.; Hasegawa, T.; Nakamura, T.; Inabe, T.; Saito, G. *Chem.−Eur. J.* **2002**, *8*, 4402.

(21) (a) Torrance, J. B.; Vazquez, J. E.; Mayerle, J. J.; Lee, V. Y. *Phys. Rev. Lett.* **1981**, *26*, 253. (b) Saito, G.; Ferraris, J. P. *Bull. Chem. Soc. Jpn.* **1980**, *53*, 2142.

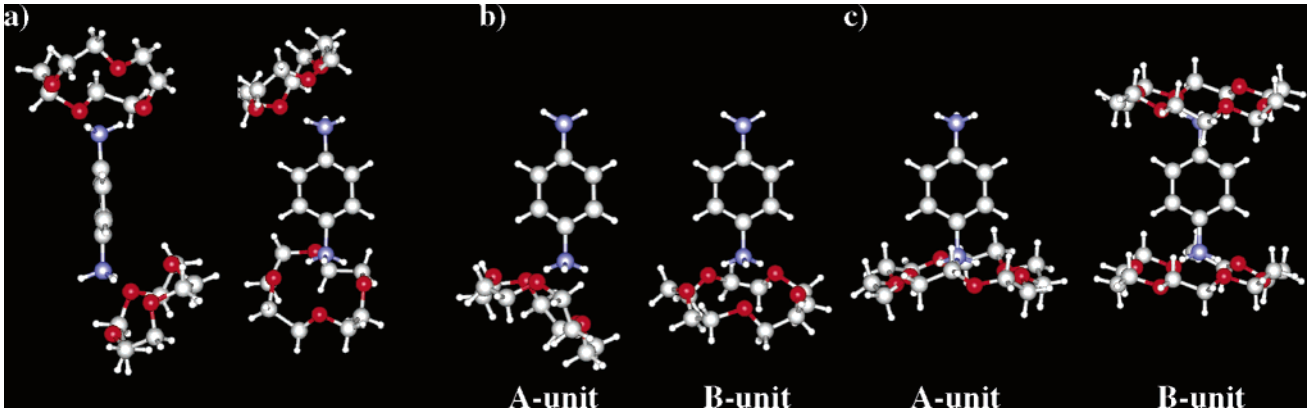

Figure 1. Supramolecular cation structures in salts **1**−**3**. (a) H_2PPD^{2+}([12]crown-4)$_2$ structure in salt **1** viewed along the short axis of H_2PPD^{2+} (left) and normal to the π plane of H_2PPD^{2+} (right). (b) Two kinds of crystallographically independent $HPPD^+$([15]crown-5) A and B units in salt **2** viewed normal to the π plane of $HPPD^+$. (c) Monocationic $HPPD^+$([18]crown-6) A unit (left) and dicationic H_2PPD^{2+}([18]crown-6) B unit (right) in salt **3** viewed normal to the π plane of PPD.

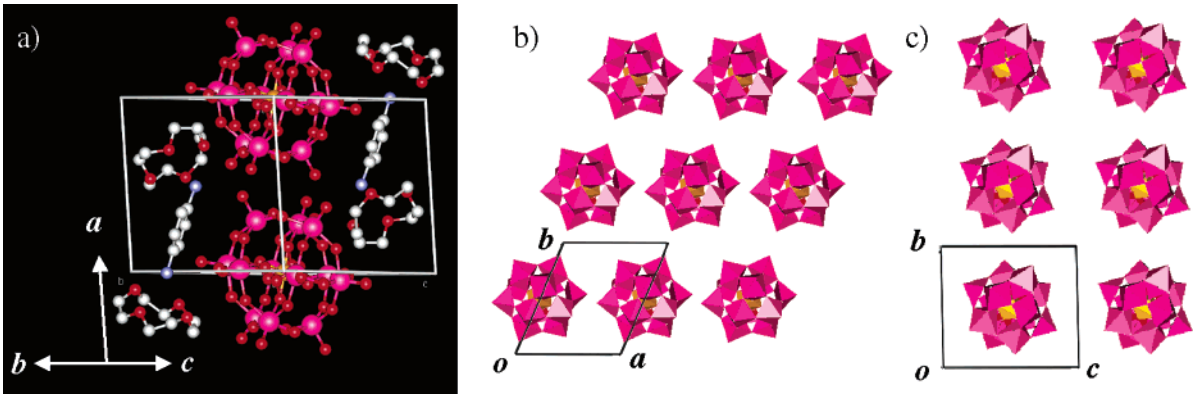

Figure 2. Crystal structure of salt **1**. (a) Unit cell viewed along the $b + c$ axis. H atoms were omitted to clarify the packing structure. Polyhedral representations of $[PMo_{12}O_{40}]^{4-}$ clusters within (b) the *ab* plane and (c) the *bc* plane.

in the A unit. It has been observed that the O atoms present in the crown ether interact strongly with the cationic $-NH_3^+$ group, as has often been observed, through H-bonded type interactions, while the affinity between the O atoms of the crown ether and the neutral $-NH_2$ group is low; this demonstrates the electrostatic nature of the interaction. As such, it can be seen that coordination between the five O atoms of [15]crown-5 and $HPPD^+$ occurred at the $-NH_3^+$ group of $HPPD^+$; the upper and lower N sites of $HPPD^+$ in Figure 1b were $-NH_2$ and $-NH_3^+$ moieties, respectively.

Both the $HPPD^+$ and $H2PPD^{2+}$ cations were confirmed in salt **3** as a $HPPD^+$([18]crown-6) A unit and a sandwich-type H_2PPD^{2+}([18]crown-6)$_2$ B unit (Figure 1c). The dihedral angles between the mean π plane of the phenyl ring and the mean O_6 plane of [18]crown-6 in the A and B units were 97° and 99°, respectively. Therefore, the long axes of the $HPPD^+$ and H_2PPD^{2+} molecules were almost normal to the O_6 plane of [18]crown-6. Both $HPPD^+$ and H_2PPD^{2+}, under Brønsted acid−base equilibrium during crystallization, were introduced into the crystal to realize a closed-packing structure of cations and anions.

The strength of $N-H^+\sim O$ hydrogen-bonded interactions of the cations in salts **1**−**3** was evaluated from the average N−O distance (d_{N-O}) between the $-NH_3^+$ group of $HPPD^+$ or H_2PPD^{2+} and the O atoms of crown ethers. The average d_{N-O} distances in salts **1**−**3** were 2.89, 2.88, and 2.92 Å, respectively, whose distances were similar to each other. The H-bonded supramolecular cation structures in salts **1**−**3** were constructed from similar magnitudes of $N-H^+\sim O$ hydrogen-bonded interactions.[22]

Packing Structures. The sandwich-type H_2PPD^{2+}([12]-crown-4)$_2$ units were arranged between $[PMo_{12}O_{40}]^{4-}$ clusters along the *a* and *b* axes (Figure 2a), where effective intermolecular interactions between cations and anions were not observed within the limit of van der Waals interactions. Parts b and c of Figure 2 show a polyhedral representation of the $[PMo_{12}O_{40}]^{4-}$ clusters forming the lattice in the *ab* and *bc* planes, respectively. Within the *ab* plane, a two-dimensional (2D) layer of $[PMo_{12}O_{40}]^{4-}$ clusters was observed. Within the *ab* plane, the P−P distances (d_{P-P}) between the nearest-neighboring $[PMo_{12}O_{40}]^{4-}$ clusters along the *a* axis (d_{P-P} = 12.1 Å) were ca. 1 and 2 Å shorter than those along the *b* axis (d_{P-P} = 13.1 Å) and along the $-a + b$ axis (d_{P-P} = 13.7 Å). The most effective intercluster interaction was observed along the *a* axis, which formed a one-dimensional (1D) chain of $[PMo_{12}O_{40}]^{4-}$ clusters. The 1D cluster chains were connected through two kinds of

(22) (a) Jeffrey, G. A. *An Introduction to Hydrogen Bonding*; Truhlar, D. G., Ed.; Oxford University Press: New York, 1997. (b) Steiner, T. *Angew. Chem., Int. Ed.* **2002**, *41*, 48.

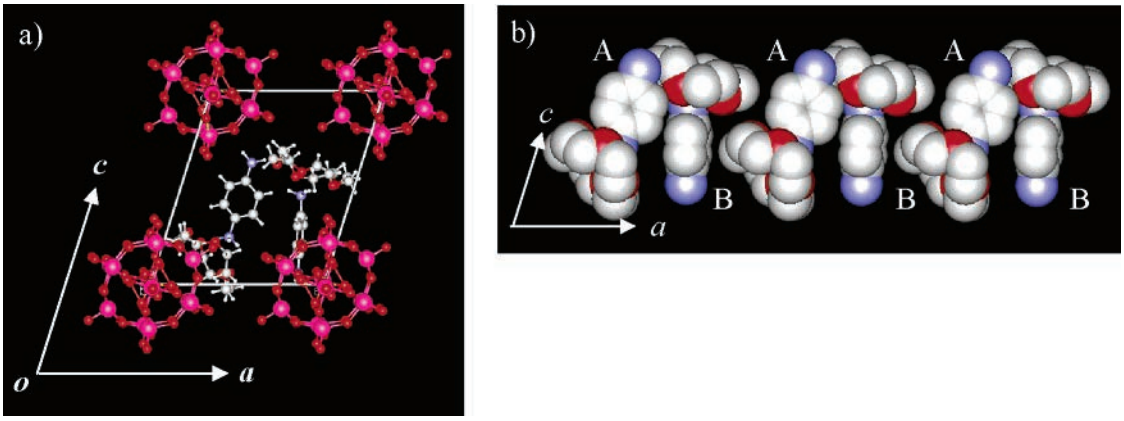

Figure 3. Crystal structure of salt **2**. (a) Unit cell viewed along the *b* axis. (b) Alternate arrangements of $HPPD^+$([15]crown-5) A and B units along the *a* axis.

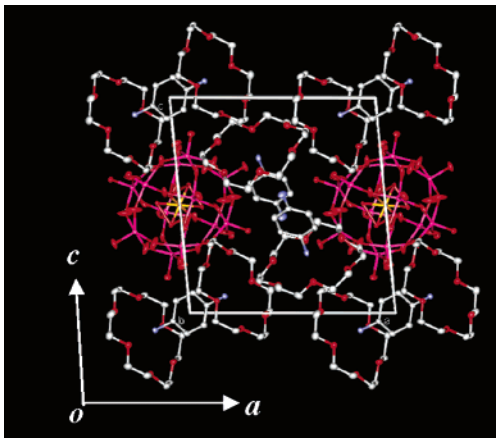

Figure 4. Crystal structure of salt **3**. Unit cell viewed along the *b* axis. H atoms were omitted for clarity.

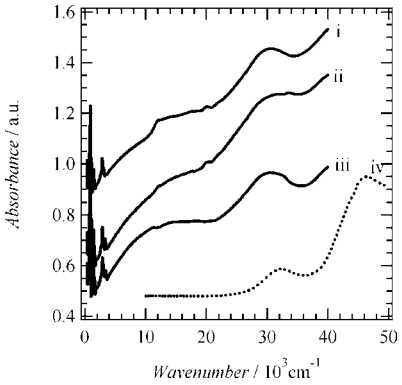

Figure 5. Electronic spectra of salts (i) **1**, (ii) **2**, and (iii) **3** on a KBr disk in addition to (iv) a solution spectrum of $(H^+)_3[PMo_{12}O_{40}]^{3-}$ in CH_3CN.

intercluster interactions along the *b* and $-a + b$ axes, forming the 2D later within the *ab* plane.

The $[PMo_{12}O_{40}]^{4-}$ clusters of salt **2** were observed on the lattice points, while the $(HPPD^+)$([15]crown-5) cations A and B formed an antiparallel dimer arrangement around the center of the unit cell (Figure 3a). Alternate arrangements of $(HPPD^+)$([15]crown-5) A and B units were observed along the *a* and *b* axes, which formed the cation layer within the *ab* plane. The cation dimer was surrounded by eight nearest-neighboring $[PMo_{12}O_{40}]^{4-}$ clusters in the crystal. The intercluster distances along the *a* axis ($d_{P-P} = 13.6$ Å) were ca. 1 and 2 Å shorter that those along the *b* axis ($d_{P-P} = 14.6$ Å) and the $-a + b$ axis ($d_{P-P} = 15.6$ Å), respectively. The 1D arrangement of the $[PMo_{12}O_{40}]^{4-}$ clusters along the *a* axis dominated intercluster interaction in salt **2**. However, the shortest intercluster distance was 1.5 Å longer than that in compound **1**, suggesting that the intercluster interactions in **2** were decreased by increasing of the size of the crown ether from [12]crown-4 to [15]crown-5.

The sandwich-type $(H_2PPD^{2+})([18]crown-6)_2$ cations of salt **3** were observed on the lattice points (Figure 4), while two $(HPPD^+)$([18]crown-6) cations existed at around the center of the unit cell. The most effective intercluster interaction was observed along the *a* axis with d_{P-P} of 14.2 Å, the distance of which was 0.4 and 0.7 Å shorter than those along the *b* and *c* axes, respectively. Because the intercluster distances in salt **3** were 1−2 Å longer than those in salt **1**, each Keggin cluster was isolated to each other because of the large size of the [18]crown-6 molecules separating the $[PMo_{12}O_{40}]^{4-}$ clusters in salt **3**.

Electronic Spectra of Salts 1−3. The electronic states of $[PMo_{12}O_{40}]^{4-}$ in salts **1**−**3** were evaluated by UV−vis−near-IR−IR spectra of the solid (Figure 5). The yellow $(H^+)_3[PMo_{12}O_{40}]^{3-}$ did not show the d−d transition (spectrum iv in Figure 5) due to the $(4d)^0$ electronic structure of the Mo^{VI} ions. The electronic absorptions at 32 and 46 × 10^3 cm^{-1} have been assigned to the metal−ligand charge-transfer electronic excitation from the doubly occupied oxo orbitals to the unoccupied d orbitals of Mo^{VI}.[23,24] On the other hand, the electronic spectra of salts **1**−**3** showed broad absorption in the vis−near-IR−IR energy region. Because the octahedral coordination of six O atoms to a Mo ion splits the d orbitals into t_{2g} and e_g orbitals, whose energy separation was usually larger than 10 × 10^3 cm^{-1}, the low-energy absorption in salts **1**−**3** was assigned to the intervalence transition from Mo^V to Mo^{VI} through the Mo−O−Mo bond within the cluster and the d−d transitions of Mo^V octahe-

(23) Pope, M. T. *Heteropoly and Isopoly Oxometalates*; Springer-Verlag: Berlin, 1983; p 109.
(24) (a) Robin, M. B.; Day, P. *Adv. Inorg. Chem. Radiochem.* **1967**, *10*, 248.

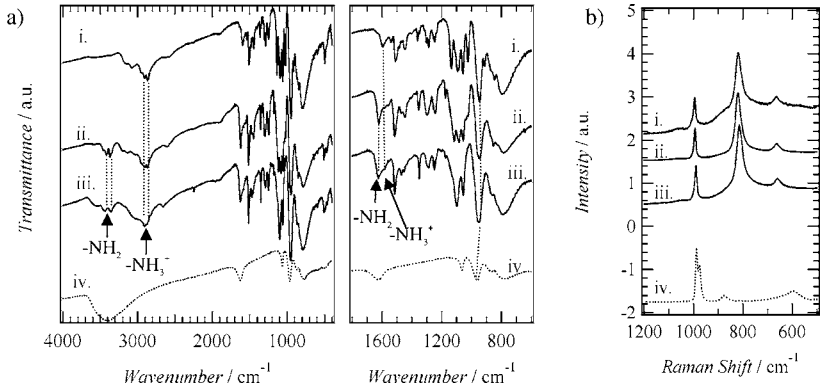

Figure 6. Vibrational spectra of salts **1**−**3** and $(H^+)_3[PMo_{12}O_{40}]^{3-}\cdot nH_2O$. (a) IR spectra of salts (i) **1**, (ii) **2**, (iii) **3**, and (iv) $(H_3^+)[PMo_{12}O_{40}]^{3-}\cdot nH_2O$ on a KBr pellet. The spectra in the energy regions 4000−400 and 1800−600 cm^{-1} are shown in the left and right figures, respectively. (b) Raman spectra of salts (i) **1**, (ii) **2**, (iii) **3**, and (iv) $(H_3^+)[PMo_{12}O_{40}]^{3-}$ on a polycrystalline sample.

dra.[9,23,24] Because the terminal Mo−O distance (d_t) of the $[PMo_{12}O_{40}]$ cluster was shorter than the inner (d_a) and bridging Mo−O distances (d_b), the $[MoO_6]$ octahedra were rather too distorted to cause further splitting of the d orbitals. Therefore, the complex and broad electronic absorption bands were observed at an energy below $\sim 18 \times 10^3$ cm^{-1}.[9]

IR and Raman Spectra of Salts 1−3. The protonated states of the PPD derivatives and the electronic states of $[PMo_{12}O_{40}]^{4-}$ in salts **1**−**3** were evaluated from the vibrational spectra (Figure 6). The N−H stretching modes (ν_{N-H}) of $-NH_2$ and $-NH_3^+$ have been typically observed at 3500−3300 and 3130−3030 cm^{-1}, respectively, while the N−H deformation modes (δ_{N-H}) of $-NH_2$ and $-NH_3^+$ were observed at around 1650−1560 and 1600 cm^{-1}, respectively.[25] In general, the energy of the vibrational bands of the $-NH_2$ group was higher than that of the $-NH_3^+$ group. The cation structure of $(H_2PPD^{2+})([12]crown\text{-}4)_2$ in salt **1** may exhibit the vibrational bands of $-NH_3^+$ only, while the IR spectra of salts **2** and **3** were expected to show both the $-NH_3^+$ and $-NH_2$ vibrational modes simultaneously. The ν_{N-H} mode of the $-NH_2$ group was not observed in the energy region around 3400 cm^{-1} for salt **1**, while those in salts **2** and **3** were clearly confirmed at 3418 and 3370 cm^{-1}, respectively (Figure 6a). The disappearance of the ν_{N-H} mode of the $-NH_2$ group in salt **1** was consistent with the formation of the sandwich-type cation structure of $(H2PPD^{2+})$-$([12]crown\text{-}4)_2$. The ν_{N-H} modes of the $-NH_3^+$ groups of $HPPD^+$ and H_2PPD^{2+} in salts **1**−**3** were observed as broad bands with two transmittance maxima observed at 2870 and 2910 cm^{-1}.

The absorptions at 1516 and 1470 cm^{-1} were assigned to the aromatic C=C stretching mode ($\nu_{C=C}$) of the phenyl ring, and those around 1100 cm^{-1} were related to the C−O−C stretching mode of the crown ethers. The δ_{N-H} mode of the $-NH_3^+$ groups for H_2PPD^{2+} in salt **1** was observed at 1597 cm^{-1}, while the δ_{N-H} mode of the $-NH_2$ group in salts **2** and **3** appeared at 1625 cm^{-1} accompanied by a shoulder of the δ_{N-H} vibrational mode of the $-NH_3^+$ group at around 1600 cm^{-1}. Because salts **2** and **3** showed δ_{N-H} modes of both the $-NH_3^+$ and $-NH_2$ groups, the monoprotonated $HPPD^+$ cations were included in the salts.

Characteristic vibrational bands of $(H^+)_3[PMo_{12}O_{40}]^{3-}$ in the IR spectrum (iv in Figure 6) were observed at 1065 and 962 cm^{-1}, which were assigned to the asymmetric coupling mode of ν_{P-O}/ν_{Mo-O} and asymmetric ν_{Mo-O} modes, respectively.[26] The asymmetric ν_{Mo-O} modes for salts **1**−**3** were observed at 946, 946, and 947 cm^{-1}, respectively, whose energy was ca. 15 cm^{-1} red-shifted from the $[PMo_{12}O_{40}]^{3-}$ cluster by one-electron reduction. The red shifts of the asymmetric ν_{Mo-O} mode in the reduced Keggin cluster have been already reported,[27] and the force constant of the Mo−O stretching mode was found to decrease by the introduction of one electron into the cluster due to electron delocalization on the cluster framework.

In the Raman spectrum of $(H^+)_3[PMo_{12}O_{40}]^{3-}$, the symmetric and asymmetric ν_{Mo-O} modes were observed at 989 and 977 cm^{-1}, respectively (spectrum iv in Figure 6b).[26b] The Raman spectra of salts **1**−**3** showed sharp symmetric vibrational modes at 995, 995, and 993 cm^{-1}, respectively. The symmetric ν_{Mo-O} mode of salts **1**−**3** was ca. 7 cm^{-1} red-shifted through the one-electron reduction of the Keggin cluster. Although the vibrational modes found around 820 cm^{-1} are related to the PPD derivatives, a clear correlation between the energy of these bands and the protonated states was not observed.

Magnetic Susceptibilities of Salts 1−3. Figure 7 shows the χ_{mol} vs T (*left* scale) and $\chi_{mol}T$ vs T (*right* scale) plots of salt **2** in the temperature range from 2 to 300 K. The temperature-dependent magnetic susceptibilities of salts **1** and **3** were also similar to that of salt **2**. The $\chi_{mol}T$ vs T plot of salt **2** was in accordance with the Curie−Weiss behavior, whose Curie constant was 0.322 emu K mol^{-1}. This value was slightly decreased from the calculated Curie constant of 0.355 emu K mol^{-1} with $g = 1.945$. Although the $C = 0.325$ emu K mol^{-1} value of salt **3** was similar to that of salt **2**, the magnetic susceptibility of salt **1** ($C = 0.258$ emu K mol^{-1}) was appreciably reduced from that of the free spin. The suppression of magnetic susceptibility in salt **1** may be

(25) Akalin, E.; Akyüz, S. *Vib. Spectrosc*. **2000**, *22*, 3.

(26) (a) Rocchiccioli-Deltcheff, C.; Fournier, M.; Franck, R.; Thouvenot, R. *Inorg. Chem*. **1983**, *22*, 207. (b) Neier, R.; Trojanwski, C.; Mattes, R. *J. Chem. Soc., Dalton. Trans*. **1995**, 2521. (c) Bridgeman, A. J. *Chem.—Eur. J*. **2004**, *10*, 2935.

(27) Rocchiccioli-Deltcheff, C.; Thouvenot, R.; Franck, R. *Spectrochim. Acta* **1975**, *32A*, 597.

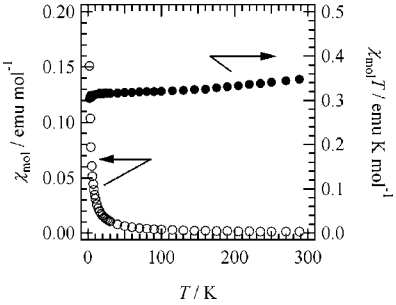

Figure 7. χ_{mol} vs T (left scale) and $\chi_{mol}T$ vs T (right scale) plots of salts **2** in polycrystalline samples. χ_{mol} of salt **2** per one $[PMo_{12}O_{40}]^{4-}$ cluster is plotted in the figure.

due to (i) spin−orbit coupling of the distorted Mo^V octahedron, (ii) antiferromagnetic interaction between $[PMo_{12}O_{40}]^{4-}$ clusters, or (iii) a slight change in the protonated state of the crystal.

When the excess protons were introduced or removed from the ideal stoichiometry of $(H2PPD^{2+})_2([12]crown\text{-}4)_4[PMo_{12}O_{40}]^{4-}$, the number of the $S = {}^1/_2$ spin on the cluster should be modified. About a 20% fluctuation of the H^+ stoichiometry of $(H^+)_{4\pm0.2}(PPD)_2([12]crown\text{-}4)_4[PMo_{12}O_{40}]^{(4\pm0.2)-}$ reduces the C value from the free spin value to 0.25 emu K mol^{-1}. Although a distinct change of the protonated states and electronic structures could not be identified from both the vibrational and electronic spectra, the possibility of a slight change in the protonated state of salt **1** should not be completely disregarded at present. The antiferromagnetic interactions between $[PMo_{12}O_{40}]^{4-}$ clusters are also expected to reduce the C value of salt **1**. In the crystal, the 2D layer and effective intercluster interactions of the $[PMo_{12}O_{40}]^{4-}$ clusters were observed. The intercluster distance in salt **1** was ca. 1−2 Å shorter than those in salts **2** and **3**, which should increase the magnetic exchange interactions between the $[PMo_{12}O_{40}]^{4-}$ clusters in salt **1**. Although the lowest unoccupied molecular orbital coefficients at terminal O atoms of the Keggin structure were quite significantly small,[28] intercluster antiferromagnetic exchange energy is expected to reduce the magnetic susceptibility of salt **1** and remains a possibility of the spin−orbit coupling of the Mo^V octahedron within the cluster.

The magnitude of the spin−orbit coupling constant (λ) for the second and third transition-metal ions is usually larger than that for the first transition-metal ions because of the d-electron broadening, which decreases the absolute magnitude of the magnetic susceptibility. The magnetic susceptibility including the spin−orbit coupling constant is expressed for the ground-state symmetry of the $[Mo^VO_6]$ octahedron ($^2T_2$) as

$$\chi_{mol} = \frac{N_A\mu_B{}^2}{3k_BT}\left[\frac{8 + \left(\frac{3\lambda}{k_BT} - 8\right)\exp\left(-\frac{3\lambda}{2k_BT}\right)}{\frac{\lambda}{k_BT}\left[2 + \exp\left(-\frac{3\lambda}{2k_BT}\right)\right]}\right] \quad (1)$$

Table 2. Average Mo−O Distances[a] and Spin−Orbit Coupling Constant (λ) in Salts **1**−**3**

	1	**2**	**3**
C, emu K mol^{-1}	0.258	0.322	0.325
λ, cm^{-1}	+589	+353	+347
d_t, Å	1.66	1.65	1.66
d_b, Å	1.90	1.90	1.89
d_a, Å	2.39	2.48	2.45

[a] The shape of the $[MoO_6]$ octahedron was evaluated from Mo−O distances of terminal Mo−O (d_t), bridging Mo−O−Mo (d_b), and anionic Mo−PO_4^{3-} (d_a).

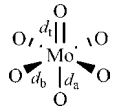

where N_A, μ_B, and k_B are Avogadro's number, the Bohr magneton, and Boltzmann's constant, respectively. The magnitude of λ is +155 cm^{-1} for a free spin and depends on a structural distortion of the $[Mo^VO_6]$ octahedron, where a large distortion of the octahedron decreased the λ value.[29] Table 2 summarizes the Curie constant (C) and spin−orbit coupling constant (λ) calculated from eq 1 of salts **1**−**3** together with the average Mo−O distances of terminal Mo−O (d_t), bridging Mo−O−Mo (d_b), and anionic Mo−PO_4^{3-} (d_a) in the $[MoO_6]$ octahedron.

The distortion of the $[MoO_6]$ octahedron was evaluated from Mo−O distances of d_t, d_b, and d_a. In salt **1**, the average distances of d_t, d_b, and d_a were 1.66, 1.90, and 2.39 Å, respectively, which were within the same range of previously reported reduced Keggin structures of $[Fe(C_5Me_5)_2]_4[PMo_{12}O_{40}]^{4-}$ and $(tetrathiafulvalene)_6(tetraethylammonium^+)(H^+)[PMo_{12}O_{40}]^{4-}$.[7b,c] Because the terminal d_t of salt **1** was ca. 0.3 and 0.7 Å shorter than the bridging d_b and anionic d_a, the $[MoO_6]$ octahedron was distorted to form an ideal octahedron. Although the lengths of d_t and d_b for salts **1**−**3** were observed within a similar range, the length of d_a for salt **1** (2.39 Å) was about 0.1 Å shorter than those of salts **2** (2.48 Å) and **3** (2.45 Å). Therefore, the structural distortion of the $[MoO_6]$ octahedron for salt **1** was smaller than those of salts **2** and **3**. Both the spin−orbit coupling on the Mo^V octahedron and antiferromagnetic interaction between $[PMo_{12}O_{40}]^{4-}$ clusters play an important role in reducing the absolute magnitude of the magnetic susceptibility in salt **1**.

Spin Dynamics in the $[PMo_{12}O_{40}]^{4-}$ Cluster. The formation of one-electron-reduced $[PMo_{12}O_{40}]^{4-}$ clusters was confirmed by temperature-dependent magnetic susceptibilities of salts **1**−**3**. One 4d electron on the $[PMo_{12}O_{40}]^{4-}$ cluster was delocalized on the cluster at room temperature from the appearance of an intervalence transition at $\sim 8 \times 10^3$ cm^{-1} in the electronic spectra, which suggested delocalization of a $S = {}^1/_2$ spin of the Mo^V ion on the cluster.[9] Figure 8a shows the ESR spectra of a polycrystalline sample of salt **2** at 5, 50, and 80 K. Because the π spin of PPD derivatives was not detected in salts **1**−**3** from ESR spectra, the closed-shell cation structures of $HPPD^+$ and H_2PPD^{2+} were confirmed.

(28) (a) Poblet, J. P.; López, X.; Bo, C. *Chem. Soc. Rev.* **2003**, *32*, 297. (b) López, X.; Maestre, J. M.; Bo, C.; Poblet, J.-M. *J. Am. Chem. Soc.* **2001**, *123*, 9571.

(29) (a) Carlin, R. L. *Magnetochemistry*; Springer-Verlag: Heidelberg, Germnay, 1986. (b) Kahn, O. *Molecular Magnetism*; VCH: New York, 1993.

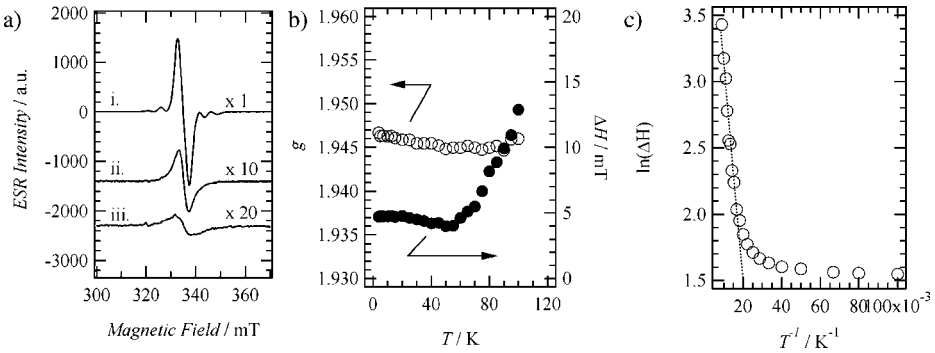

Figure 8. Temperature-dependent ESR spectra of salt **2**. (a) ESR signals of a polycrystalline sample of salt **2** at (i) 5 K (×1), (ii) 50 K (×10), and (iii) 80 K (×20), respectively. (b) Temperature-dependent *g* value (left scale) and Δ*H* value (right scale) in the temperature range from 4 to 100 K. The *g* values were corrected by a MnO marker. (c) ln(Δ*H*) vs T^{-1} plot.

A Lorentzian-type ESR spectrum at $g = 1.946$ and a line width (Δ*H*) of 4.73 mT was observed at 5 K, while the *g* value and Δ*H* at 80 K were observed at 1.945 and 8.17 mT, respectively. Weak hyperfine structures around both sides of the central signal at $g = 1.946$ were due to the two isotopes of ^{95}Mo and ^{97}Mo species with a nuclear spin of $I = {}^5/_2$. The intensity of the ESR signals of salt **2** followed the Curie−Weiss law, which was consistent with the temperature-dependent magnetic susceptibility. Figure 8b shows the temperature-dependent *g* values (*left* scale) and Δ*H* (*right* scale) of salt **2**. The *g* values showed the temperature-independent behavior from 4 to 100 K, while an abrupt enhancement of the Δ*H* values was observed by increasing the temperature at around 60 K. The magnitude of Δ*H* at 100 K (12.89 mT) was about 3 times larger than that at 50 K (4.00 mT), and the change in Δ*H* has been discussed from a motional freedom of one $S = {}^1/_2$ spin on a reduced $[PMo_{12}O_{40}]^{4-}$ cluster. The temperature-dependent Δ*H* values of the Keggin cluster were composed of the sum of temperature-independent ΔH_0 and temperature-dependent ΔH_T as expressed in eq 2, where the ΔH_T term is proportional to the hopping frequency (ν_T) of the $S = {}^1/_2$ spin between the nearest-neighboring Mo sites.[30]

$$\Delta H = \Delta H_0 + \Delta H_T = \Delta H_0 + C\nu_T \qquad (2)$$

The ν_T term can be further expressed by Mott's hopping frequency as[31]

$$\nu_T = \nu_0 \exp(-2\alpha R) \exp(-E_{th}/k_B T) \qquad (3)$$

where α, *R*, and E_{th} are the tunneling factor, nearest-neighboring Mo−Mo distance, and activation energy of spin dynamics, respectively. Because ν_0, α, and *R* are constants, the ln Δ*H* vs T^{-1} plots yield E_{th} of spin dynamics within the reduced $[PMo_{12}O_{40}]^{4-}$ cluster (Figure 8c). The E_{th} value was 0.015 eV for salt **2** in the temperature range from 60 to 120 K, which was similar to those previously reported.[9a] The spin in the cluster was localized at a specific Mo^V site in the temperature range below 60 K, while the spin had a motional freedom among the 12 Mo sites above 60 K.

(30) (a) Movaghar, B.; Schweitzer, L.; Overhof, H. *Philos. Mag. B* **1978**, *37*, 683. (b) Bachus, R.; Movaghar, B.; Schweitzer, L.; Voget-Grote, U. *Philos. Mag. B* **1979**, *39*, 27.

(31) (a) Austin, I. G.; Mott, N. F. *Adv. Phys.* **1969**, *18*, 41. (b) Mott, N. F. *Metal−Insulator Transition*, 2nd ed.; Taylor & Francis: New York, 1990.

Summary

Supramolecular cation structures between protonated PPD derivatives of $HPPD^+$ and/or H_2PPD^{2+} and crown ethers of [12]crown-4, [15]crown-5, and [18]crown-6 were introduced into the one-electron-reduced α-$[PMo_{12}O_{40}]^{4-}$ Keggin salts. Three new Keggin salts of $(H_2PPD^{2+})_2$([12]crown-4)$_4$-$[PMo_{12}O_{40}]^{4-}$ (**1**), $(HPPD^+)_4$([15]crown-5)$_4[PMo_{12}O_{40}]^{4-}$ (**2**), and $(HPPD^+)_2(H_2PPD^{2+})$([18]crown-6)$_4[PMo_{12}O_{40}]^{4-}(CH_3CN)_4$ (**3**) were successfully obtained by the electron- and proton-transfer processes between the electron donor (proton acceptor) of PPD and the electron acceptor (proton donor) of the $(H^+)_3[PMo_{12}O_{40}]^{3-}$ clusters. The cation structure in salt **1** was the sandwich-type (H_2PPD^{2+})([12]crown-4)$_2$, while that in salt **2** was the monoprotonated 1:1 $(HPPD^+)$([15]-crown-5) adduct. The mono- and diprotonated states of $(HPPD^+)$([18]crown-6) and (H_2PPD^{2+})([18]crown-6)$_2$ coexisted in salt **3**. Because the coordination affinity of the O atoms of crown ethers for the amino group was negligible in general, the sandwich-type coordination corresponded to the formation of the H_2PPD^{2+} state in salts **1** and **3**, and the 1:1 adduct between $HPPD^+$ and crown ethers was formed in salts **2** and **3**. The Brønsted acid−base equilibrium and formation of a closed-packing structure in the crystals yielded different types of cationic structures and molecular assemblies in salts **1**−**3**. A 2D layer of $[PMo_{12}O_{40}]^{4-}$ clusters was observed in salt **1**, in which 1D $[PMo_{12}O_{40}]^{4-}$ chains were connected through interchain interactions. On the other hand, the clusters in salts **2** and **3** were isolated from each other. By an increase in the size of the crown ethers, the magnitude of intercluster interactions decreased in the order of [12]crown-4, to [15]crown-5, to [18]crown-6 because of an increase of the cation volume in the crystals. The crystals were fundamentally constructed from the electrostatic interaction between $[PMo_{12}O_{40}]^{4-}$ tetravalent anions and supramolecular cations. The crystal densities of salts **1**−**3** decreased in the order of the size of the crown ethers, and CH_3CN molecules were introduced into salt **3** in order to fill the crystal space. Therefore, the cation size of $(H2PPD^{2+})$-([12]crown-4)$_2$ was just fitted to the formation of a closed-packing structure of $[PMo_{12}O_{40}]^{4-}$ tetravalent anions in the

crystal. One-electron-reduced α-$[PMo_{12}O_{40}]^{4-}$, bearing one $S = {}^1/_2$ spin, was confirmed by the temperature-dependent magnetic susceptibilities of salts **1**−**3**. The electronic absorption spectra of salts **1**−**3** revealed the intervalence optical transition between the pentavalent Mo^V and hexavalent Mo^{VI} ions within the cluster. In addition, temperature-dependent ESR spectra of salt **2** showed delocalization of the $S = {}^1/_2$ spin on the cluster above 60 K. The localization−delocalization spin transition was observed at 60 K by a temperature-dependent line width of the ESR spectra. The controls of spin dynamics and intervalence electron transfer within the reduced Keggin clusters have the potential of forming novel electrical and magnetic materials of an organic−inorganic hybrid molecular system.

Acknowledgment. This work was partly supported by a Grant-in-Aid for Scientific Research from the Ministry of Education, Culture, Sports, Science and Technology of Japan.

Supporting Information Available: Crystal data (CIF) of salts **1**−**3**, selected bond lengths, temperature-dependent magnetic susceptibilities of salts **1** and **3**, cyclic voltammetry, XRD, and TG−DTA chart of salt **3**. This material is available free of charge via the Internet at http://pubs.acs.org.

IC060857I